Agile and Dynamic Standing-up Control for Humanoids using 3D Divergent Component of Motion in Multi-contact Scenario

Grazia Zambella[1], Robert Schuller[2], George Mesesan[2], Antonio Bicchi[1,3], Christian Ott[2,4], and Jinoh Lee[2,5]

***Abstract*— Standing-up is a task that humanoids need to be able to perform in order to be employed in real-world scenarios. This paper proposes a new robust strategy for a humanoid to stand up in challenging scenarios where no completely preplanned motion can accomplish the same task. This strategy exploits the concept of three-dimensional divergent component of motion and passivity-based whole-body control. The latter firstly maximizes the push forces applied to the robot's center of mass to make agile whole-body recovery motion. Then, during the rising phase, it reduces these forces to zero and stabilizes the robot in an upward position. Optimization of centroidal angular momentum is fully integrated into the proposed whole-body standing-up control to create the trajectories of the hip and the upper body joints online. The effectiveness of the proposed method is validated in simulations and experiments on the humanoid TORO.**

I. Introduction

Thanks to their anthropomorphic shape, humanoid robots are able to perform balancing, locomotion, and manipulation tasks. Therefore, they can be employed in different applications such as manufacturing, healthcare, education, or search and rescue. All these applications make humanoids very appealing to several research groups. Indeed, many researchers have focused on the design of new control approaches to balance this kind of robots also in challenging scenarios [1]–[3]. Other research groups developed new technologies for humanoids' safe interaction with people and with the environment [4], [5]. Many others studied new planning algorithms that allow these robots to perform tasks in a partially or fully autonomous way [6]–[8]. Among the myriad of autonomous tasks, standing up is a crucial capability that humanoids must possess in order to be employed in any of the aforementioned real-world applications.

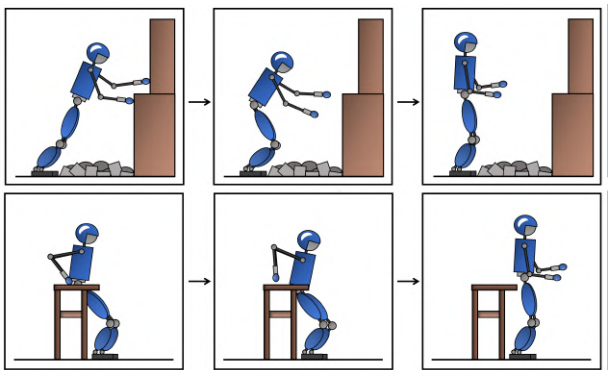

Fig. 1. Examples of dynamic standing-up to recover the upward position for seamless autonomous operations in real-world scenarios.

In literature, standing-up is tackled in a static or dynamic way. Machine learning is one of the many techniques to generate standing-up motion. For example, in [9], exploiting the humanoids' bilateral symmetry, authors apply the Q-learning method to design an optimal policy for the standing-up motion for DarwIn-OP humanoid. In [10]–[13], learning from demonstration approaches are adopted to reproduce humans' dynamic movements of sit-to-standing and roll-and-rise. While those techniques exhibit significant potential, implementation necessitates a training phase, which, if conducted in simulations, demands precise model knowledge to transfer the result to the hardware; alternatively, training on the physical robot may pose a risk of damage.

In contrast, model-based approaches obviate training, yet generally entail complete preplanning of standing-up motion. In [14], an iterative system identification framework is proposed to design reference trajectories performing lean-to-stand, sit-to-stand, kneel-to-stand, and stand-to-handstand, with model parameterization and control optimization. Authors in [15] study possible transitions towards different stable poses to design predictable motions that allow a quadruped humanoid to recover itself after a fall. A more recent work of [16] proposes a method to generate fast and reliable standing-up motion based on quintic spline interpolation to recover humanoids after a fall, while authors in [17] show preplanned trajectories for standing-up motion corrected online according to any change in the environment and of the robot state.

However, preplanning the standing-up motion is not always possible, particularly due to sudden contact transitions.

Manuscript received 21 March 2023; accepted 4 July 2023; published 19 July 2023. This paper was recommended for publication by Editor A. Kheddar upon evaluation of the Associate Editor and Reviewers' comments. This work was supported in part by the European Union's Horizon 2020 Research and Innovation Programme under Grants 871237 (SOPHIA) and 101070596 (euROBIN), and in part by the European Research Council (ERC) Programme under Grant 819358 (NatDyReL). (*Corresponding author: Grazia Zambella*)

[1]Authors are with the Centro di Ricerca "E. Piaggio" and the Dipartimento di Ingegneria dell'Informazione, Università di Pisa, 56122 Pisa, Italy. (e-mail: gr.zambella@gmail.com).

[2]Authors are with Institute of Robotics and Mechatronics, German Aerospace Center (DLR), 82234 Weßling, Germany (e-mails: {robert.schuller, george.mesesan, jinoh.lee}@dlr.de).

[3]Author is also with the Soft Robotics for Human Cooperation and Rehabilitation, Istituto Italiano di Tecnologia, Genova 16163, Italy (e-mail: antonio.bicchi@unipi.it).

[4]Author is also with Institut für Automatisierungs, Technische Universität Wien, 1040 Wien, Austria (e-mail: christian.ott@tuwien.ac.at).

[5]Author is also with the Department of Mechanical Engineering, Korea Advanced Institute of Science & Technology (KAIST), Daejeon, Korea.

Digital Object Identifier (DOI): see top of this page.

For example, during search and rescue operations, the humanoid will face challenging environments and manipulate in critical configurations, from which it can stand up only in a dynamic way without completely preplanned motion, i.e., it can stand up only moving through different contact configurations without maintaining contacts throughout the motion (Fig. 1). There has been recent literature tackling this type of scenario. Authors in [18] introduce a dynamic whole-body control strategy for the agile standing-up based on the total energy of center-of-mass (CoM) dynamics. During the push phase, contact wrenches are computed to satisfy inequality constraints (e.g, friction cone, torque limits, etc.) which ensure that the energy generated is sufficient to accelerate the robot's CoM as quickly as possible; the acquired energy is then controlled to facilitate a rapid raising-up and balance in the upright position. This approach offers the advantage of obviating the need for a preplanned CoM motion during the push phase. However, the switching time between the two phases, which coincides with the hands detachment time, is determined empirically. This makes this approach heuristic.

Whereas interestingly, authors in [19] present an analytic approach to plan and control online multi-contact motions for humanoid robots based on the 3D-Divergent Component of Motion (DCM) concept. The planner takes a sequence of multi-contact stances and computes the timing of contact transitions on-the-fly and the references for the end-effectors considering the feasibility of the motion with respect to kinematic and dynamic constraints. The 3D-DCM control is then integrated with the passivity-based whole-body controller [1] to track these planned trajectories. Therefore, this approach presents the advantage of inheriting the robustness of the passivity-based whole-body control framework, but it requires to design the CoM motion since it places Virtual Repellent Point (VRP) positions for each contact configuration.

In this paper, we propose a novel method for humanoids to perform the standing-up in an agile, dynamic, yet robust manner without using completely preplanned motion. In particular, leveraging the robustness to robot model uncertainties, the ease of tuning, and suitability to multi-contact scenarios, we exploit the passivity-based whole-body control approach [19] in the first phase to exert maximum forces for pushing the CoM, and then in the second phase, to diminish these forces to zero for decelerating the CoM motion and stabilizing the robot in the upright position.

The proposed method is distinguishable with the following contributions: i) unlike [18], the time to switch the phases of the standing-up motion is not heuristically determined but online-planned based on the 3D-DCM; and ii), to generate online the waist orientation and the upper body joints motion after hands detachment, the proposed method integrates centroidal angular momentum (CAM) optimization from [20]. In particular, the design of the reference for this optimizer has two purposes: to reduce the disturbing effect of the CAM on the CoM motion during the first phase (i.e., regulating the CAM to zero), and to actively generate CAM during the second phase to support the rising motion of the humanoid.

II. Fundamentals

Here, we provide a brief overview of the humanoid's dynamic model and a summary of the previous works on the passivity-based whole-body controller [1], [20]–[22].

A. Dynamic Model

The humanoid robot is modeled as a floating base robot with n torque-controlled joints. The floating base is described using the position of the CoM $\boldsymbol{x}_c \in \mathbb{R}^3$ and the orientation of the waist $\boldsymbol{R}_b \in SO(3)$, and the corresponding translational and rotational velocities $\dot{\boldsymbol{x}}_c \in \mathbb{R}^3$, and $\boldsymbol{\omega}_b \in \mathbb{R}^3$. Therefore, the system's total number of degrees of freedom (DoFs) is $\bar{n} = n+6$. Defining $\boldsymbol{\nu}_c = (\dot{\boldsymbol{x}}_c^T \ \boldsymbol{\omega}_b^T)^T$, and $\boldsymbol{q} \in \mathbb{R}^n$ as the joint position vector, the dynamics of the system is written as

$$\boldsymbol{M}\begin{pmatrix} \dot{\boldsymbol{\nu}}_c \\ \ddot{\boldsymbol{q}} \end{pmatrix} + \boldsymbol{C}\begin{pmatrix} \boldsymbol{\nu}_c \\ \dot{\boldsymbol{q}} \end{pmatrix} + \begin{pmatrix} -\boldsymbol{w}_g \\ \boldsymbol{0} \end{pmatrix} = \begin{pmatrix} \boldsymbol{0} \\ \boldsymbol{\tau} \end{pmatrix} + \boldsymbol{\tau}_{ext}, \quad (1)$$

where $\boldsymbol{M} \in \mathbb{R}^{\bar{n}\times\bar{n}}$ denotes the inertia, $\boldsymbol{C} \in \mathbb{R}^{\bar{n}\times\bar{n}}$ the Coriolis matrix, $\boldsymbol{\tau} \in \mathbb{R}^n$ the joint torques vector, $\boldsymbol{w}_g = (m\boldsymbol{g}_0^T \boldsymbol{0}^T)^T$ the gravitation wrench (m is the overall robot mass and $\boldsymbol{g}_0 \in \mathbb{R}^3$ is the vector of gravitational acceleration), and $\boldsymbol{\tau}_{ext} \in \mathbb{R}^{\bar{n}}$ the generalized external forces acting on the system. To formulate a model suitable for a balancing controller, the joint coordinates of the feet and of the hands, the latter only if in contact with the environment, are substituted by their Cartesian coordinates. Hence, denoting with $n_h \in \{1,2\}$ the number of the hands in contact with the environment, $\boldsymbol{\nu} \in \mathbb{R}^{12+6n_h}$ is defined as the velocity vector that stacks the translational and rotational velocity, $\dot{\boldsymbol{x}}_i \in \mathbb{R}^3$ and $\boldsymbol{\omega}_i \in \mathbb{R}^3$ respectively, of the feet and, according to the situation, of one or both the hands. Indicating with $\dot{\boldsymbol{q}}_f \in \mathbb{R}^{n-12-6n_h}$ the remaining free DoFs defined in joint space, the Jacobian $\boldsymbol{J} \in \mathbb{R}^{\bar{n}\times\bar{n}}$ that maps into task space velocities $\dot{\boldsymbol{x}} \in \mathbb{R}^{\bar{n}}$ is computed as

$$\underbrace{\begin{pmatrix} \boldsymbol{\nu}_c \\ \boldsymbol{\nu} \\ \dot{\boldsymbol{q}}_f \end{pmatrix}}_{\dot{\boldsymbol{x}}} = \underbrace{\begin{bmatrix} \boldsymbol{I} & \boldsymbol{0} \\ \boldsymbol{Ad} & \boldsymbol{J}' \\ \boldsymbol{0} & \boldsymbol{S}_f \end{bmatrix}}_{\boldsymbol{J}} \begin{pmatrix} \boldsymbol{\nu}_c \\ \dot{\boldsymbol{q}} \end{pmatrix}, \quad (2)$$

where $\boldsymbol{S}_f \in \mathbb{R}^{(n-12-6n_h)\times n}$ is the matrix that selects the joints corresponding to $\dot{\boldsymbol{q}}_f$ from whole joint vector, and, as shown in [22], $\boldsymbol{Ad} \in \mathbb{R}^{(12+6n_h)\times 6}$ and $\boldsymbol{J}' \in \mathbb{R}^{(12+6n_h)\times n}$ are respectively the stacked adjoint matrices and the stacked Jacobians.

B. Passivity-based Whole-body Controller

The passivity-based whole-body controller computes joint torque commands generating reaction forces for the robot to accomplish the desired movement and to reject external disturbances. For simplicity, the derivation presented in this subsection assumes that the robot is in full contact with the environment. However, the formulation is extendable to the other contact configurations.

Considering $\dot{\boldsymbol{x}}^{cmd}$ the robot's desired motion in the task space, the corresponding commanded CoM and joint trajectories are computed via inverse kinematics from (2)

$$\begin{pmatrix} \boldsymbol{\nu}_c^{cmd} \\ \dot{\boldsymbol{q}}^{cmd} \end{pmatrix} = \boldsymbol{J}^{-1}\dot{\boldsymbol{x}}^{cmd}. \quad (3)$$

By defining $\Delta\boldsymbol{\nu} = \boldsymbol{\nu}_c - \boldsymbol{\nu}_c^{cmd}$ and $\Delta\dot{\boldsymbol{q}} = \dot{\boldsymbol{q}} - \dot{\boldsymbol{q}}^{cmd}$, inspired by PD+ control [23], the desired closed-loop system is given as

$$\boldsymbol{M}\begin{pmatrix}\Delta\dot{\boldsymbol{\nu}}_c\\ \Delta\ddot{\boldsymbol{q}}\end{pmatrix}+\boldsymbol{C}\begin{pmatrix}\Delta\boldsymbol{\nu}_c\\ \Delta\dot{\boldsymbol{q}}\end{pmatrix}=\boldsymbol{\tau}_{ext}-\boldsymbol{J}^T\begin{pmatrix}\boldsymbol{w}_c^{imp}\\ \boldsymbol{w}_{ct,f}\\ \boldsymbol{w}_{ct,h}\\ \boldsymbol{\tau}_f^{imp}\end{pmatrix}, \quad (4)$$

where $\boldsymbol{w}_c^{imp} \in \mathbb{R}^6$ represents the CoM impedance wrench, $\boldsymbol{w}_{ct,f} \in \mathbb{R}^{12}$ and $\boldsymbol{w}_{ct,h} \in \mathbb{R}^{12}$ denote concatenated contact wrenches of both feet and hands, respectively, and $\boldsymbol{\tau}_f^{imp}$ is the impedance torque vector of the joint task. In particular, $\boldsymbol{w}_c^{imp} \in \mathbb{R}^6$ is computed as

$$\boldsymbol{w}_c^{imp}=\begin{pmatrix}\boldsymbol{K}_c(\boldsymbol{x}_c-\boldsymbol{x}_c^{cmd})+\boldsymbol{D}_c(\dot{\boldsymbol{x}}_c-\dot{\boldsymbol{x}}_c^{cmd})\\ \boldsymbol{\tau}_r(\boldsymbol{\Sigma}_b,(\boldsymbol{R}_b^{cmd})^T\boldsymbol{R}_b)+\boldsymbol{B}_b(\boldsymbol{\omega}_b-\boldsymbol{\omega}_b^{cmd})\end{pmatrix}, \quad (5)$$

where $\boldsymbol{\tau}_r(\boldsymbol{\Sigma}_b,(\boldsymbol{R}_b^{cmd})^T\boldsymbol{R}_b)$ denotes the virtual rotational spring controlling the waist orientation [21], $\boldsymbol{K}_c$ and $\boldsymbol{\Sigma}_b$ linear and rotational stiffness matrices, $\boldsymbol{D}_c$ and $\boldsymbol{B}_b$ damping matrices, and all gain matrices are symmetric and positive definite.

Subtracting the system dynamics (1) from the desired closed-loop behavior (4), $\bar{n}$ equations are obtained with the upper six equations describing the underactuated centroidal dynamics and the last n equations describing the dynamics of the actuated joints. The first six equations, given as

$$\boldsymbol{A}\boldsymbol{d}^T\begin{pmatrix}\boldsymbol{w}_{ct,f}\\ \boldsymbol{w}_{ct,h}\end{pmatrix}=\underbrace{\boldsymbol{M}_c\begin{pmatrix}\dot{\boldsymbol{\nu}}_c^{cmd}\\ \ddot{\boldsymbol{q}}^{cmd}\end{pmatrix}+\boldsymbol{C}_c\begin{pmatrix}\boldsymbol{\nu}_c^{cmd}\\ \dot{\boldsymbol{q}}^{cmd}\end{pmatrix}}_{\boldsymbol{w}_c^{ff}}-\boldsymbol{w}_g+\boldsymbol{w}_c^{imp}, \quad (6)$$

where the right-hand side denotes the desired CoM wrench with the feedforward term $\boldsymbol{w}_c^{ff}$, are used to compute the distribution of $\boldsymbol{w}_{ct,f}$ and $\boldsymbol{w}_{ct,h}$ in all possible configurations[1] (please refer to the details in [1].) Once the wrench distribution is obtained, joint torque commands are finally computed from the dynamic equations of the actuated joints as follows:

$$\boldsymbol{\tau}=\overbrace{\boldsymbol{M}_q\begin{pmatrix}\dot{\boldsymbol{\nu}}_c^{cmd}\\ \ddot{\boldsymbol{q}}^{cmd}\end{pmatrix}+\boldsymbol{C}_q\begin{pmatrix}\boldsymbol{\nu}_c^{cmd}\\ \dot{\boldsymbol{q}}^{cmd}\end{pmatrix}}^{\boldsymbol{\tau}_{ff}}-(\boldsymbol{J}')^T\begin{pmatrix}\boldsymbol{w}_{ct,f}\\ \boldsymbol{w}_{ct,h}\end{pmatrix} \quad (7)$$
$$-\boldsymbol{S}_f^T\boldsymbol{\tau}_f^{imp}.$$

C. Whole-body Motion Optimizer

In [20], a whole-body motion optimizer is proposed to find the optimized velocities of k selected DoFs of $\boldsymbol{q}_f$ to induce a desired CAM to the system, as indicated as a yellow block in Fig. 2. More in detail, assuming that $\boldsymbol{J}$ (2) is a square matrix and invertible[2], the CAM $\boldsymbol{l}_c \in \mathbb{R}^3$ is computed as

$$\boldsymbol{l}_c=\boldsymbol{A}\begin{pmatrix}\boldsymbol{\nu}_c\\ \dot{\boldsymbol{q}}\end{pmatrix}=\underbrace{\boldsymbol{A}\boldsymbol{J}^{-1}}_{\bar{\boldsymbol{A}}}\dot{\boldsymbol{x}}, \quad (8)$$

where $\boldsymbol{A} \in \mathbb{R}^{3\times\bar{n}}$ is the rotational part of the centroidal momentum matrix [24]. The whole task space, $\dot{\boldsymbol{x}}$, can be divided into k DoFs adjusted within the motion optimizer ($\dot{\boldsymbol{x}}_a^T \in \mathbb{R}^k$) and the remaining $\bar{n}-k$ DoFs kept unchanged with $k \in \{0,..,\bar{n}\}$ ($\dot{\boldsymbol{x}}_u^T \in \mathbb{R}^{(\bar{n}-k)}$), i.e., $\dot{\boldsymbol{x}} = \begin{bmatrix}\dot{\boldsymbol{x}}_a^T & \dot{\boldsymbol{x}}_u^T\end{bmatrix}^T$. According to (2), $\dot{\boldsymbol{x}}_u$ will always contain $\boldsymbol{\nu}_c$ and $\boldsymbol{\nu}$.

[1]Inertia and Coriolis matrices are separated into two parts: i) the upper six rows describing the centroidal dynamics, i.e., $\boldsymbol{M}_c$ and $\boldsymbol{C}_c \in \mathbb{R}^{6\times\bar{n}}$, and ii) the lower part describing the joint dynamics, i.e., $\boldsymbol{M}_q$ and $\boldsymbol{C}_q \in \mathbb{R}^{n\times\bar{n}}$.

[2]If J is a non-square matrix, a pseudo-inverse of J can be used in (8).

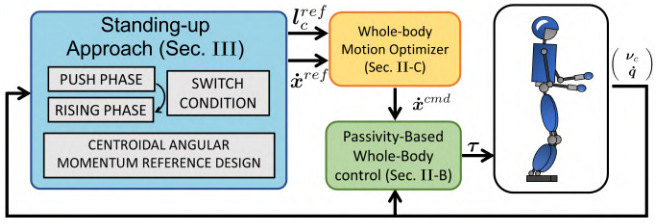

Fig. 2. Control block diagram of the proposed standing-up method in the whole-body control framework.

Defining $\boldsymbol{l}_c^{ref}$ as the predefined reference CAM to induce to the system and $\bar{\boldsymbol{A}}_a \in \mathbb{R}^{3\times k}$ and $\bar{\boldsymbol{A}}_u \in \mathbb{R}^{3\times(\bar{n}-k)}$ as the sub-matrices of $\bar{\boldsymbol{A}}$ relative to $\dot{\boldsymbol{x}}_a$ and $\dot{\boldsymbol{x}}_u$ respectively, a QP is formulated to determine the optimized $\dot{\boldsymbol{x}}_a^{opt}$ that i) satisfy

$$\boldsymbol{l}_c^{ref}=\bar{\boldsymbol{A}}_a\dot{\boldsymbol{x}}_a^{opt}+\bar{\boldsymbol{A}}_u\dot{\boldsymbol{x}}_u^{ref}, \quad (9)$$

with $\dot{\boldsymbol{x}}_u^{ref}$ the reference velocity of the unchanged DoFs, and ii) reduce the error between the optimized posture $\boldsymbol{x}_a^{opt}$ and its reference $\boldsymbol{x}_a^{ref}$ provided by the trajectory planner, i.e.,

$$\dot{\boldsymbol{x}}_a^{opt}=\dot{\boldsymbol{x}}_a^d=\dot{\boldsymbol{x}}_a^{ref}+\boldsymbol{K}_p(\boldsymbol{x}_a^{ref}-\boldsymbol{x}_a^{opt}), \quad (10)$$

with the diagonal and positive definite matrix, $\boldsymbol{K}_p$. The convergence behavior of the robot towards its reference pose is influenced by the choice of the elements of $\boldsymbol{K}_p$.

D. Definition of DCM and VRP

The 3D-DCM ($\boldsymbol{\xi}$), as presented in [25], is an extension of the 2D-DCM along the z-axis (i.e., along the axis aligned with gravity). It is defined as the linear combination of the CoM position and velocity: $\boldsymbol{\xi} = \boldsymbol{x}_c + b\dot{\boldsymbol{x}}_c$, where b is a time constant formulated as $b = \sqrt{\Delta z/g}$ with Δz the average CoM height w.r.t. the ground surface and represents the unstable part of CoM dynamics, while the VRP is formulated as the following linear combination of CoM position and acceleration: $\boldsymbol{\upsilon} = \boldsymbol{x}_c - b^2\ddot{\boldsymbol{x}}_c$.

III. Proposed Method

The proposed strategy, depicted in a blue block in Fig. 2, creates the online reference for the whole-body motion optimizer (Sec. II-C), and, consequently, for the passivity-based whole-body control, shown in Sec. II-B. The method presents two phases: the push and rising phases. During the push phase, the robot is considered to have established multiple contacts with the environment as seen in Fig. 1. Then, when the switch condition between the push and rising phases is verified, hands in contact will detach, and the robot will assume a double support configuration. If the arms reach the singularity during the push phase, the hands will detach before the rising phase starts. Consequently, it will assume the double support configuration is already in the push phase.

For brevity of the notation, we consider in the derivation that the inertial frame $\{I\}$ is placed as shown in Fig. 3a, in the middle of the feet with the z-axis perpendicular to

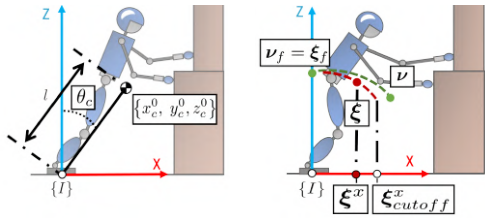

(a) (b)

Fig. 3. (a) the humanoid simplified model and its variable used during the push phase; (b) the concept behind the switch condition.

the ground and the x-axis perpendicular to the wall. In addition, according to Fig. 2, the superscript ref indicates the reference for the whole-body motion optimizer and the superscript cmd indicates the commands sent to the passivity-based whole-body control. Note that, for the CoM, the reference and the commanded trajectories coincide because the velocity of the CoM belongs to the velocities that the whole-body motion optimizer does not change.

A. Push phase

The push motion is designed along the sagittal plane of the humanoid, x- and z-axes, and along the y-axis, it is commanded zero position, velocity, and acceleration.

Along the x-axis, we want to generate with the passivity-based whole-body control the distribution of $\boldsymbol{w}_{ct,f}$ and $\boldsymbol{w}_{ct,h}$ that allows to push as much as possible the CoM towards the support area made by the feet (Fig. 3a). This is translated into commanding a constant CoM acceleration a^{ref} of large amplitude $K > 0$ with opposite sign w.r.t. x_c^0, i.e.,

$$a^{ref} = -\text{sign}(x_c^0)K\,. \tag{11}$$

Based on (6), $\ddot{x}_c^{ref} = \ddot{x}_c^{cmd} = a^{ref}$ implies $\boldsymbol{w}_{c,x}^{ff} \neq 0$, we command a null impedance wrench in order to not disturb the push motion. According to (5), making null the x component of the CoM impedance wrench $\boldsymbol{w}_c^{imp}$ corresponds with commanding CoM velocity and position, $\dot{x}_c^{ref} = \dot{x}_c^{cmd}$ and $x_c^{ref} = x_c^{cmd}$ respectively, equal to the current ones, $\dot{x}_c$ and x_c.

Along the z-axis, we exploit the inverted pendulum model to design the CoM commanded trajectory. Therefore,

$$\begin{cases} z_c^{ref} = l\,\cos\theta_c, \\ \dot{z}_c^{ref} = -l\,\sin\theta_c\dot{\theta}_c, \\ \ddot{z}_c^{ref} = -l\left(\sin\theta_c\ddot{\theta}_c + \cos\theta_c\dot{\theta}_c^2\right), \end{cases} \tag{12}$$

where l is the length of the pendulum at the time t_0 and

$$\theta_c = \arcsin\left(x_c/l\right) \tag{13}$$

is the pendulum angle w.r.t. the z-axis as seen in Fig. 3a.

B. Switch Condition

The switch condition between the push phase and the rising phase is based on the concept of the 3D-DCM. In particular, we need to check if the current DCM $\boldsymbol{\xi}$ is already on a trajectory that allows the robot to recover the upward position in a certain time $\bar{T}$. If this condition is verified and the push phase is not stopped, the humanoid will fall on its back because it is no longer possible to decelerate the CoM motion and stabilize the robot in the final position.

To derive the switch condition, we start with the formulation of the DCM trajectory. As shown in [26], the initial DCM $\boldsymbol{\xi}_0$ allowing to reach the final VRP, $\boldsymbol{v}_{\bar{T}}$, and the final DCM, $\boldsymbol{\xi}_{\bar{T}}$, in a time $\bar{T}$ can be computed as

$$\boldsymbol{\xi}_0 = \alpha\,\boldsymbol{v}_0 + \beta\,\boldsymbol{v}_{\bar{T}} + \gamma\boldsymbol{\xi}_{\bar{T}}\,, \tag{14}$$

where $\boldsymbol{v}_0$ is the initial VRP and α, β,and γ are positive coefficients whose sum is equal to 1. Considering that the final VRP and the final DCM coincide ($\boldsymbol{v}_{\bar{T}} = \boldsymbol{\xi}_{\bar{T}}$), i.e., the final DCM is stationary and is equal to the final position of the CoM, and considering the convexity property of the coefficients, (14) is simplified to

$$\boldsymbol{\xi}_0 = \alpha\,\boldsymbol{v}_0 + (1-\alpha)\,\boldsymbol{v}_{\bar{T}}\,. \tag{15}$$

Therefore, given the current VRP, $\boldsymbol{v}$, and final standing-up VRP, $\boldsymbol{v}_\text{f}$, it is possible to compute the initial DCM, $\boldsymbol{\xi}_{cutoff}$, from which $\boldsymbol{v}_\text{f}$ can be reached in a chosen time $\bar{T}$ as follows:

$$\boldsymbol{\xi}_{cutoff} = \alpha\boldsymbol{v} + (1-\alpha)\boldsymbol{v}_\text{f}\,. \tag{16}$$

If x component of the current DCM, $\boldsymbol{\xi}^x$, and the final VRP, $\boldsymbol{v}_\text{f}^x$, are on the same side w.r.t. $\boldsymbol{\xi}_{cutoff}^x$ (Fig. 3b), i.e., if

$$(\boldsymbol{\xi}_{cutoff}^x - \boldsymbol{\xi}^x)(\boldsymbol{\xi}_{cutoff}^x - \boldsymbol{v}_\text{f}^x) > 0, \tag{17}$$

the current DCM is already on the trajectory that allows the robot to reach the final position in the time $\bar{T}$. Therefore, the push phase is stopped, the push forces decrease in the x- axis and the CoM motion decelerates in order to balance in the end the robot in the upward position. Note that this condition is evaluated only for the x component because the push motion takes place on the x-axis.

C. Rising Phase

The rising phase is the last one of the standing-up procedure and aims at stabilizing the humanoid in the upward position. Therefore, w.r.t. the inertial frame $\{I\}$, on the x- and y-axes, we command zero CoM position, velocity, and acceleration. Consequently, $\boldsymbol{v}_\text{f}^x = \boldsymbol{v}_\text{f}^y = \boldsymbol{\xi}_\text{f}^x = \boldsymbol{\xi}_\text{f}^y = 0$. Instead, on the z-axis, according to (15),

$$z_{c,\text{f}}^{ref} = \boldsymbol{\xi}_\text{f}^z = \boldsymbol{v}_\text{f}^z = \boldsymbol{v}_0^z + (\boldsymbol{\xi}_0^z - \boldsymbol{v}_0^z)/(1-\alpha), \tag{18}$$

where $\boldsymbol{\xi}_0^z$ and $\boldsymbol{v}_0^z$ represent respectively the DCM and the VRP component along the z-axis at the initial time of the this phase.

D. Centroidal Angular Momentum Reference Design

During the standing-up motion, a properly generated CAM trajectory can support the desired movements. For this reason, we decide to exploit the motion optimizer presented in Sec. II-C to adjust the waist orientation and the arms' trajectory w.r.t. a CAM $\boldsymbol{l}_c^{ref}$ that we want to induce to the system and that is designed as follows. It is important to specify that the waist orientation trajectory is adjusted from the beginning and the arms one after the hands detachment.

In the push phase, we want the CAM of the system to be null ($\boldsymbol{l}_c^{ref} = 0$) not to disturb the motion by generating further wrenches at the CoM. According to (9), $\boldsymbol{l}_c^{ref} = 0$ implies

$$\bar{\boldsymbol{A}}_a\dot{\boldsymbol{x}}_a^{opt} = -\bar{\boldsymbol{A}}_u\dot{\boldsymbol{x}}_u^{ref}\,, \tag{19}$$

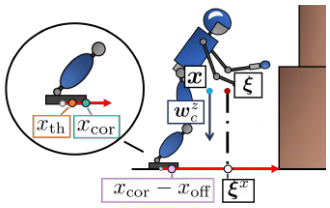

Fig. 4. The description of variables used for the design of the CAM references during the rising phase.

i.e., the optimizer will overwrite the velocity of the k DoFs that the motion optimizer can adjust to produce a CAM that is opposite to the one induced by the unchanged $\bar{n}-k$ DoFs. Note that, if the robot is fully in contact, $\dot{\boldsymbol{x}}_a^{opt}$ consists of the rotational velocity of the waist. When the hands detach and the humanoid switches in the double support configuration, $\dot{\boldsymbol{x}}_a^{opt}$ also includes the arm joint velocities.

During the rising phase, we want to induce the CAM that helps to stabilize the humanoid in the upward position. This means that the generated CAM will first help to push the DCM, and, consequently, the CoM, inside the support polygon. Once it is inside, the CAM will help to decelerate the CoM motion. Note that, since in this phase the robot is in the double support configuration, the support polygon corresponds to the convex hull of the feet. Moreover, considering that the rising motion happens along the x- and z-axes, and also that the DCM is already within the support polygon of the robot along the y-axis, only the y component of $\boldsymbol{l}_c^{ref}$ ($\boldsymbol{l}_{c,y}^{ref}$) needs to be designed to support the motion in x-direction. The other two components, $\boldsymbol{l}_{c,x}^{ref}$ and $\boldsymbol{l}_{c,z}^{ref}$, since the rising motion is supposed to be symmetrical in the y and z plane, are regulated to zero. For the design of $\boldsymbol{l}_{c,y}^{ref}$, indicating with x_{cor} half of the length of the feet (Fig. 4) and x_{off} an offset that reduces the support polygon to be safe, if $|\boldsymbol{\xi}_x| \geq x_{\text{cor}} - x_{\text{off}}$, i.e., the DCM is outside the support polygon, we design a torque τ_y^{ref}, and the corresponding rate of change of CAM ($\dot{\boldsymbol{l}}_{c,y}^{ref}$), that pushes the DCM inside the support polygon. Therefore, indicating with $\boldsymbol{w}_c^z$ the z-axis component of the current CoM wrench calculated from the distribution of $\boldsymbol{w}_{ct,f}$ and $\boldsymbol{w}_{ct,h}$ obtained solving the QP of the passivity-based whole-body control, based on [27], we formulate τ_y^{ref} as

$$\tau_y^{ref} = -\left(x_{\text{cor}} - x_{\text{off}} - \boldsymbol{\xi}^x\right) \boldsymbol{w}_c^z \,. \tag{20}$$

Then, if $x_{\text{th}} \leq |\boldsymbol{\xi}_x| \leq x_{\text{cor}} - x_{\text{off}}$, where $x_{\text{th}} > 0$ is a threshold, we design $\tau_y^{ref} = 0$. This phase is introduced to avoid the DCM being directly pushed outside the reduced support area again. In particular, reducing the CAM (negative torque) deflects the DCM in the opposite direction to the desired one. Therefore, with the threshold, we ensure that the DCM is already within the support area considering a certain safety margin. There, a small deviation induced by the reduction of CAM is not activating the first phase (20) again. In the end, if the DCM is close enough to the center of the support polygon, i.e., $x_{\text{th}} > |\boldsymbol{\xi}_x|$, we want to cancel completely the centroidal angular momentum. To do this, we apply a second-order control law to compute $\dot{\tau}_{y,t}^{ref}$, i.e.,

$$\dot{\tau}_y^{ref} = -K_d^l \tau_y^{ref} - K_p^l \boldsymbol{l}_{c,y}^{ref} \tag{21}$$

with $K_d^l, K_p^l > 0$ and, then, we compute τ_y^{ref} by Euler integration method. Once τ_y^{ref} is computed, for each phase, $\boldsymbol{l}_{c,y}^{ref}$ to induce to the system is obtained integrating τ_y^{ref}.

IV. Validation

To validate the proposed approach, we applied it to the torque-controlled humanoid robot TORO [28], a 27 DoFs robot with a mass of 79.2kg and a height of 1.74m. We tested the method in simulation with OpenHRP [29] and in real experiments. (Please also refer to the supplementary video.)

A. Practical Implementation

First, we define the hands as point contacts and the feet as surface contacts. To fully exploit the system's potential, we integrate the torque constraints in the passivity-based whole-body control. In this way, we relax the constraint regarding the maximum normal force of hand contact to push as much as possible in all configurations. Defining $\bar{\boldsymbol{\tau}}$ as the vector whose components are the maximum torque of each joint, from (7), we can formulate the torque constraints as

$$-\bar{\boldsymbol{\tau}} - \boldsymbol{\tau}^{ff} + \boldsymbol{S}_f^T \boldsymbol{\tau}_f^{imp} \leq -(\boldsymbol{J}')^T \begin{pmatrix} \boldsymbol{w}_{ct,f} \\ \boldsymbol{w}_{ct,h} \end{pmatrix} \leq \bar{\boldsymbol{\tau}} - \boldsymbol{\tau}^{ff} + \boldsymbol{S}_f^T \boldsymbol{\tau}_f^{imp} \,. \tag{22}$$

For safety reasons, we set $\bar{\boldsymbol{\tau}}$ equal to 75% of the real maximum torque vector. Moreover, for the hand contact, we set $f_\perp = 1000$N in simulation, but only 50N in the real scenario due to the hardware limitations of the real robot.

Then, for the CAM optimizer, we implement two different QP problems: one for the "full-in-contact" configuration and one for the double support one. To ensure the continuity of the reference trajectory during the motion, the double support optimizer is initialized with the last value computed in the QP of the full in-contact configuration. The block that computes the reference, l_c^{ref}, is the same for both the QP problems. In particular, to compute l_c^{ref}, we set $x_{\text{cor}} = 0.08$ m, $x_{\text{off}} = 0.02$ m, $x_{\text{th}} = 0.05$ m, $K_d^l = 20\frac{1}{s}$ and $K_p^l = 100\frac{1}{s^2}$.

For the implementation of the standing-up approach, we implement an observer to estimate the current position and the velocity of the CoM necessary for the push phase and to compute the switch condition. At the time t, we obtain the current CoM wrench, $\boldsymbol{w}_c$, from the $\boldsymbol{w}_{ct,f}$ and $\boldsymbol{w}_{ct,h}$ computed by the QP of the passivity-based whole-body control. Dividing $\boldsymbol{w}_c$ by the total mass of the robot, we estimate the CoM acceleration $\ddot{\boldsymbol{x}}_{c,t}^{est}$. Then, the estimated velocity $\dot{\boldsymbol{x}}_{c,t}^{est}$ is computed by integrating

$$\ddot{\boldsymbol{x}}_{c,t}^{est} + K_d \left(\dot{\boldsymbol{x}}_{c,t}^{meas} - \dot{\boldsymbol{x}}_{c,t-T}^{est}\right), \tag{23}$$

where $\dot{\boldsymbol{x}}_{c,t}^{meas}$ is the measured velocity of the CoM, T is the sampling time and $K_d > 0$ (we take $K_d = 25\frac{1}{s}$). For the position, as done for the velocity,

$$\dot{\boldsymbol{x}}_{c,t}^{est} + K_p \left(\boldsymbol{x}_{c,t}^{meas} - \boldsymbol{x}_{c,t-T}^{est}\right) \tag{24}$$

with $K_p > 0$ (we tune $K_p = 10\frac{1}{s}$), is integrated.

Moreover, to avoid jumps in joint torques when the push phase starts, we made smooth $\ddot{x}_c^{ref}$, (11). In particular, indicating with t_0 the initial time of the push, we command

$$\ddot{x}_c^{ref} = -\text{sign}(x_c) K (t - t_0)/(t - t_0 + K_t), \tag{25}$$

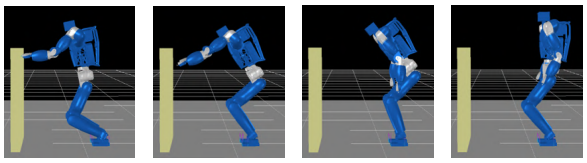

(a) t= 0.1 s (b) t= 0.59 s (c) t= 1.5 s (d) t= 5 s

Fig. 5. The dynamic simulation with the proposed standing-up control.

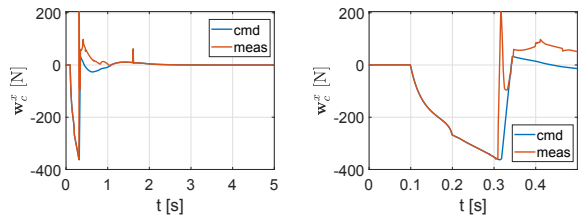

(a) whole duration t=0-5s (b) push-rising phases (t=0-0.5s)

Fig. 6. Plots of CoM wrench in x-axis and its focused view for t=0-0.5s.

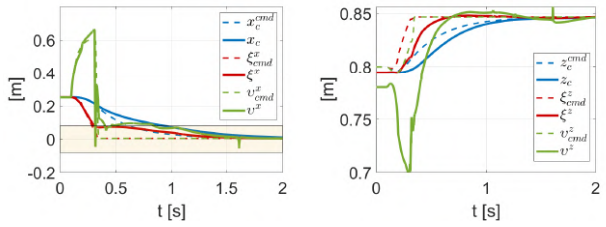

(a) x-axis (b) z-axis

Fig. 7. Tracking during the simulation: dashed lines are the commanded trajectories and solid lines are the measured ones. The yellow area in (a) indicates the support polygon area of the feet when hands detach.

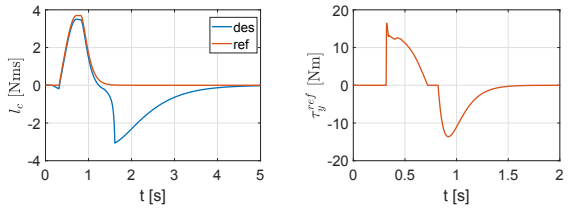

(a) (b)

Fig. 8. (a) the reference of CAM l_c^{ref}, and the desired CAM produced by the optimizer; and (b) the response of the time derivative of l_c^{ref}, i.e., τ_y^{ref}.

where K_t is a positive small number (we set $K_t = 0.05$ s) and K, as shown in Sec. III-A, is a positive number. We take $K = 5\frac{m}{s^2}$ (the corresponding force is obtained by multiplying for the mass of the robot, i.e., 396 N). Finally, if $\ddot{x}_{c,t}^{est}$ is saturated, we also saturate $\ddot{x}_c^{ref}$ to the current value because the maximum that the system can do has already been reached.

B. Simulation Results

1) Wall-assisted standing-up: In this simulation, we show the proposed method's efficiency, particularly when the arms reach the singularity and, consequently, the hands detach during the push phase. TORO's initial configuration is shown in Fig. 5a. Considering the origin of $\{I\}$ in the middle of the feet as shown in Sec. III, this configuration corresponds to CoM initial position $\boldsymbol{x}_{c,0} = [0.251\ 0.0\ 0.79]^T$m, right hand position $\boldsymbol{x}_{rh,0} = [0.9\ \ -0.3\ \ 1.0]^T$m and left hand position

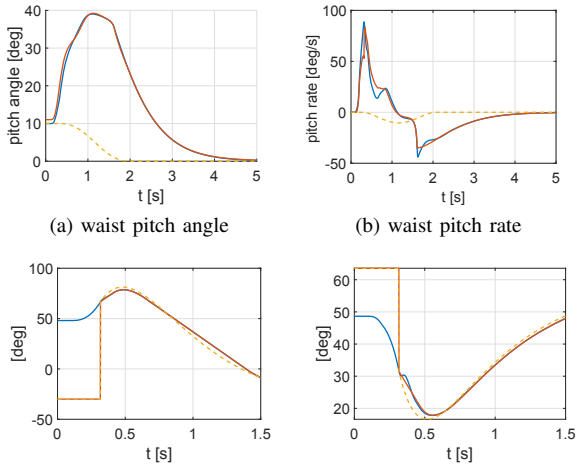

(a) waist pitch angle (b) waist pitch rate

(c) right shoulder angle (d) right elbow angle

Fig. 9. The plots of waist and arm motions, where the dashed yellow line represents reference trajectories of the joints position; the red line is commanded trajectories of joints position obtained by optimizing the CAM, and the blue line is the measured one (the plot of the left arm is omitted due to similarity to the right arm.) Note that the joint position trajectories are obtained by integrating $\dot{\boldsymbol{x}}^{ref}$ and $\dot{\boldsymbol{x}}^{cmd}$.

$\boldsymbol{x}_{lh,0} = [0.9\ 0.3\ 1.0]^T$m.

At 0.1 s, the standing-up is commanded, and the push phase starts. This is visible in Fig.6 and, more in detail, in Fig.6b where we report the desired wrench $\boldsymbol{w}_c^{cmd}$ (the blue line) and $\boldsymbol{w}_c$ (red line) along the x-axis. As explained before, at each time step, the switch condition is controlled, (17), and it is also checked if the arms are close to the singularity. This is determined by observing the elbow joint position, and the threshold for this joint is set at 40 deg. In this simulation, the singularity of the arms that forces the hands' detachment occurs at 0.31 s. Indeed, in Fig.6b, we can notice that, at this moment, since no wrenches can be generated from the hands anymore, $\boldsymbol{w}_c^x$ (red line in the plot), i.e., the current CoM wrench along the x-axis computed from $\boldsymbol{w}_{ct,f}$ and $\boldsymbol{w}_{ct,h}$, is not following the desired one. Instead, the switch condition holds at 0.32 s. The rising phase starts, and the absolute value of $\boldsymbol{w}_c^{cmd,x}$ decreases to 0. In Fig.6b, we can also see that the maximum amplitude of $\boldsymbol{w}_c^x$, in the push phase, is equal to 360.7 N. Consequently, dividing this value by the mass of TORO, we obtained the maximum CoM acceleration along the x-axis, $\ddot{x}_c$, equal to $4.55\frac{m}{s^2}$. Moreover, the maximum speed reached in the push phase, $\dot{x}_c$, is equal to $0.4364\frac{m}{s}$, which is almost its twice walking speed in a general condition [30].

Fig. 7 reports the CoM position, the DCM, and the VRP evolution during the standing-up (continuous lines) and the desired trajectories for all these variables (dashed lines). In the beginning, for the x-axis, we can see that the tracking is good, but it gets worse when the hands detach, and no wrenches can be generated from the hands anymore. For the z-axis, the tracking is not satisfying. This is due to two factors: i) we set the passivity-based QP gains higher for the CoM angular momentum than for the CoM forces; ii) while the push motion along the x-axis is helped by the CAM, the motion on the z-axis could fall into conflict with it. Nevertheless, in the end, all the variables converge to

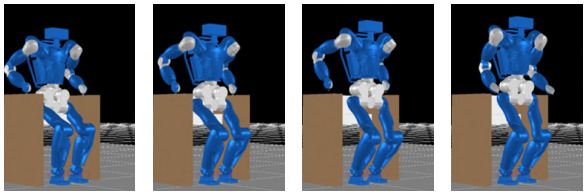

(a) t= 0.1 s (b) t= 0.56 s (c) t= 1 s (d) t= 2.5 s

Fig. 10. Simulation of the dynamic standing up from a sitting position.

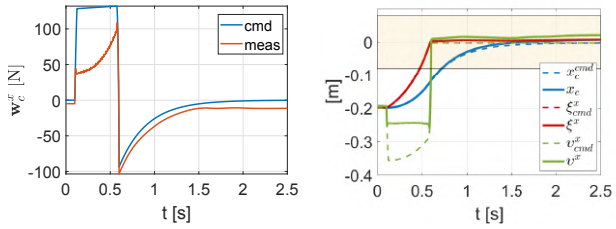

(a) CoM wrench in x-axis (b) tracking along x-axis

Fig. 11. The plots of control results, where dashed lines are the commanded trajectories, and solid lines are the measured ones. The yellow region in (b) indicates the support polygon area of the feet when hands detach.

the desired one. It is important to underline that the bad tracking does not influence the computation of $\boldsymbol{\xi}_{cutoff}$ and the evaluation of the switch condition. The latter, indeed, depends on $\boldsymbol{\xi}^x$, and on $\boldsymbol{v}^x_{\mathrm{f}}$ that is stationary.

As shown in Fig. 8, the whole-body motion optimizer is active during all standing-up motions. It overwrites from the beginning the commanded trajectory for the waist orientation (especially for the pitch angle, Figs. 9a and 9b) and, after the detachment, also the arms' joint trajectory (Figs. 9c and 9d). Thus, in Fig. 9, one can observe the trajectory generated by optimizing the CAM (continuous red line) is different from the planned one (dashed yellow line). Moreover, Fig. 8b shows the evolution of τ_y^{ref} computed as shown in Sec. III-D. During the push phase, i.e., between 0.1-0.32 s, $\boldsymbol{l}_c^{ref} = 0$. When the rising phase starts, as shown in Fig. 7, the DCM is outside the support polygon. The torque is thus computed as in (20). From 0.72 s to 0.82 s, the relation $x_{\mathrm{th}} \leq |\boldsymbol{\xi}_x| \leq x_{\mathrm{cor}} - x_{\mathrm{off}}$ holds and $\tau_y^{ref} = 0$. As a result, the CAM is constant. After $t = 0.82$ s, the absolute value of the DCM is less than the threshold x_{th}, and the τ_y^{ref} commanded to the optimizer, (21), is such that to reduce $\boldsymbol{l}_c^{ref}$ that goes to zero.

2) Standing-up from a chair: To present the validity of the proposed method in a different scenario, we perform the standing-up from a chair (Fig. 10). TORO's initial configuration, shown in Fig. 10a, corresponds to CoM initial position $\boldsymbol{x}_{c,0} = [-0.2\ 0.0\ 0.86]^T$m, right hand position $\boldsymbol{x}_{rh,0} = [-0.2\ -0.35\ 0.84]^T$m and left hand position $\boldsymbol{x}_{lh,0} = [-0.2\ 0.35\ 0.84]^T$m, expressed in the inertial frame $\{I\}$. As seen in Fig. 11a, at 0.1s, standing-up is commanded, and the push phase starts. Then, at 0.57s, the switch condition holds, and the rising phase starts. Since arms are kept in non-singular configurations, the hands detach with the rising phase. In 1.5s, the robot is stable in the upward position (Fig. 11b). In this case, while the tracking of the CoM position and the DCM is good, the one of the VRP and the wrench is not satisfying in the push phase. This is caused by the

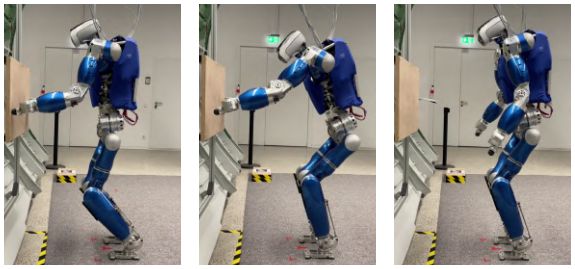

(a) t = 0 s (b) t = 0.53 s (c) t = 1.64 s

Fig. 12. Snapshots of the standing-up experiment on the real robot, TORO.

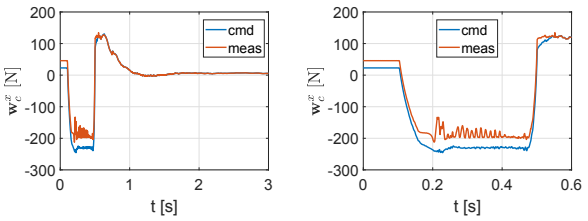

(a) whole duration t=0-3s (b) push-rising phases (t=0-0.6s)

Fig. 13. The CoM wrench in x-axis during the standing-up experiment.

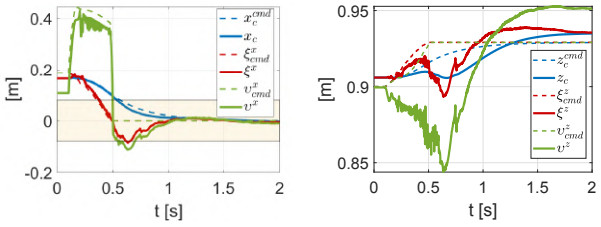

(a) x-axis (b) z-axis

Fig. 14. Tracking during the experiment: dashed lines are the commanded trajectories and solid lines are the measured ones. The transparent yellow area in (a) indicates the support polygon area of the feet when hands detach.

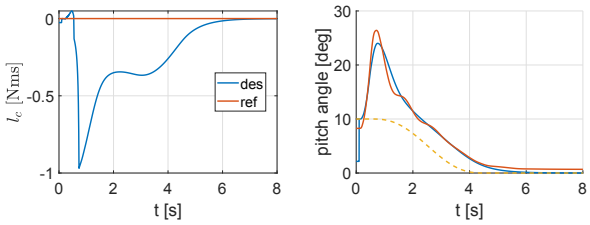

(a) (b)

Fig. 15. (a) the CAM trajectory: the red line corresponds to l_c^{ref} and the blue one is the optimized l_c; and (b) waist pitch angle responses: the dashed yellow line is the reference trajectory, the red solid line the commanded trajectory given optimizing the CAM, and the blue line the measured one.

torque constraints in the QP optimization of the passivity-based whole-body controller (22). Indeed, the torques at elbow joints are saturated, and thus it is not possible to push more.

C. Experimental Results

The experiment we carried out was less challenging than the one in the simulation. Indeed, the limitation mentioned above on the maximum force with which each arm can push (i.e., 50 N) narrowed the range of the possible TORO's initial configurations for the experiment. In this range, we have chosen the initial configuration with the CoM as far away as possible from the middle of the feet (Fig. 12a).

This configuration corresponds to CoM initial position $\boldsymbol{x}_{c,0} = [0.18\ 0\ 0.9]^T$m, right hand position $\boldsymbol{x}_{rh,0} = [0.65\ -0.3\ 1]^T$m, and left hand position $\boldsymbol{x}_{lh,0} = [0.65\ 0.3\ 1]^T$m.

As shown in Figs. 13 and 14, and more in detail in Fig. 13b, the standing-up motion starts at $t = 0.1$ s. In this case, the arms never reach a configuration close to the singularity. For this reason, the hands detach when the rising phase starts, i.e., at $t = 0.47$ s. In Fig.13b, we can notice that the absolute value of $\boldsymbol{w}_c^{cmd,x}$, from that moment, decreases to 0. Unlike the simulation, where the CoM is pushed with a force of maximum amplitude equal to 360.7 N (Fig. 6), the maximum force applied to the CoM is 194 N. This is due to the limitation on the hand's contact maximum normal force.

Moreover, as shown in Fig. 15, the whole-body motion optimizer is active during all the standing-up motion. In Fig. 15a, we notice that the designed CAM reference is always equal to zero since the rising phase starts when the measured DCM is already less than x_{th}. Fig. 15b shows how the whole-body motion optimizer overwrites the trajectory for the pitch angle from the beginning of the motion.

V. Conclusion

In this paper, we propose a new whole-body control strategy for humanoids to perform agile standing-up. This approach consists of two phases: push and rising. During the push phase, the passivity-based whole-body control is exploited to maximize the push forces applied to the CoM in a stable manner. In the rising phase, the same whole-body controller is used to stabilize the CoM in the upward position. The decision to switch from the push phase to the rising phase is taken online using the terminal condition based on the 3D-DCM concept. The CAM control is integrated to facilitate online adjustment of the waist orientation and the joint motion of the arms when the hands are detached. Therefore, this approach offers the benefits of circumventing preplanned CoM motion during the push phase, dynamically creating the motion of the waist and arms in real-time, and analytically computing the switch time. The simulation results using the humanoid TORO demonstrate the efficacy of the approach even when the arms encounter singularity, resulting in the detachment of hands during the push phase. The experimental results showcase the feasibility of the proposed method with a real full-body humanoid robot.

Acknowledgement

The authors would like to thank Dr. Johannes Englsberger for his valuable suggestions.

References

[1] B. Henze, *et al.*, "Passivity-based whole-body balancing for torque-controlled humanoid robots in multi-contact scenarios," *Int. J. Robot. Res.*, vol. 35, no. 12, pp. 1522–1543, 2016.

[2] O. Khatib, *et al.*, "A unified framework for whole-body humanoid robot control with multiple constraints and contacts," in *European Robotics Symposium*. Springer, 2008, pp. 303–312.

[3] E. Farnioli, *et al.*, "Toward whole-body loco-manipulation: Experimental results on multi-contact interaction with the walk-man robot," in *IEEE/RSJ Int. Conf. Intell. Robots Syst.*, 2016, pp. 1372–1379.

[4] F. Negrello, *et al.*, "A modular compliant actuator for emerging high performance and fall-resilient humanoids," in *IEEE-RAS Int. Conf. Humanoid Robots*, 2015, pp. 414–420.

[5] M. Grebenstein, *et al.*, "The DLR hand arm system," in *Int. Conf. Robot. Autom.*, 2011, pp. 3175–3182.

[6] M. Murooka, *et al.*, "Humanoid loco-manipulation planning based on graph search and reachability maps," *IEEE Robot. Autom. Lett*, vol. 6, no. 2, pp. 1840–1847, 2021.

[7] Q. Zhu, *et al.*, "Autonomous narration of humanoid robot kitchen task experience," in *IEEE-RAS Int. Conf. Humanoid Robots*, 2017, pp. 390–397.

[8] A. Paolillo, *et al.*, "Autonomous car driving by a humanoid robot," *Journal of Field Robotics*, vol. 35, no. 2, pp. 169–186, 2018.

[9] H. Jeong *et al.*, "Efficient learning of stand-up motion for humanoid robots with bilateral symmetry," in *IEEE/RSJ Int. Conf. Intell. Robots Syst.*, 2016, pp. 1544–1549.

[10] M. Mistry, *et al.*, "Sit-to-stand task on a humanoid robot from human demonstration," in *IEEE-RAS Int. Conf. Humanoid Robots*, 2010, pp. 218–223.

[11] M. Gonzalez-Fierro, *et al.*, "Full-body postural control of a humanoid robot with both imitation learning and skill innovation," *Int. J. Humanoid Robotics*, vol. 11, no. 02, p. 1450012, 2014.

[12] M. González-Fierro, *et al.*, "A humanoid robot standing up through learning from demonstration using a multimodal reward function," in *IEEE-RAS Int. Conf. Humanoid Robots*, 2013, pp. 74–79.

[13] Y. Kuniyoshi, *et al.*, "Embodied basis of invariant features in execution and perception of whole-body dynamic actions—knacks and focuses of roll-and-rise motion," *Robotics and Autonomous Systems*, vol. 48, no. 4, pp. 189–201, 2004.

[14] J. Tan, *et al.*, "Simulation-based design of dynamic controllers for humanoid balancing," in *IEEE/RSJ Int. Conf. Intell. Robots Syst.*, 2016, pp. 2729–2736.

[15] J. A. Castano, *et al.*, "Design a fall recovery strategy for a wheel-legged quadruped robot using stability feature space," in *IEEE Int. Conf. on Robotics and Biomimetics (ROBIO)*, 2019, pp. 41–46.

[16] S. Stelter, *et al.*, "Fast and reliable stand-up motions for humanoid robots using spline interpolation and parameter optimization," in *Int. Conf. on Advanced Robotics (ICAR)*, 2021, pp. 253–260.

[17] L. Rossini, *et al.*, "Loco-manipulation planning for legged robots: Offline and online strategies," *arXiv preprint arXiv:2205.10277*, 2022.

[18] Y. Lee, *et al.*, "Agile standing-up control of humanoids: Energy-based reactive contact wrench optimization with strict dynamic consistency," in *IEEE/RSJ Int. Conf. Intell. Robots Syst.*, 2019, pp. 4652–4659.

[19] G. Mesesan, *et al.*, "Dynamic multi-contact transitions for humanoid robots using divergent component of motion," in *Int. Conf. Robot. Autom.*, 2017, pp. 4108–4115.

[20] R. Schuller, *et al.*, "Online centroidal angular momentum reference generation and motion optimization for humanoid push recovery," *IEEE Robot. Autom. Lett*, vol. 6, no. 3, pp. 5689–5696, 2021.

[21] C. Ott, *et al.*, "Posture and balance control for biped robots based on contact force optimization," in *IEEE-RAS Int. Conf. Humanoid Robots*, 2011, pp. 26–33.

[22] G. Mesesan, *et al.*, "Dynamic walking on compliant and uneven terrain using DCM and passivity-based whole-body control," in *IEEE-RAS Int. Conf. Humanoid Robots*, 2019, pp. 25–32.

[23] B. Paden *et al.*, "Globally asymptotically stable 'PD+'controller for robot manipulators," *Int. J. Cont.*, vol. 47, no. 6, pp. 1697–1712, 1988.

[24] D. E. Orin, *et al.*, "Centroidal dynamics of a humanoid robot," *Autonomous robots*, vol. 35, no. 2–3, pp. 161–176, Oct. 2013.

[25] J. Englsberger, *et al.*, "Three-dimensional bipedal walking control based on divergent component of motion," *IEEE Transactions on Robotics*, vol. 31, no. 2, pp. 355–368, 2015.

[26] G. Mesesan, *et al.*, "Convex properties of center-of-mass trajectories for locomotion based on divergent component of motion," *IEEE Robot. Autom. Lett*, vol. 3, no. 4, pp. 3449–3456, 2018.

[27] M. Popovic, "Ground reference points in legged locomotion: Definitions, biological trajectories and control implications," *The Int. J. Robot. Res.*, vol. 24, pp. 1013–1032, 12 2005.

[28] J. Englsberger, *et al.*, "Overview of the torque-controlled humanoid robot TORO," in *IEEE-RAS Int. Conf. Humanoid Robots*, 2014, pp. 916–923.

[29] F. Kanehiro, *et al.*, "Openhrp: Open architecture humanoid robotics platform," *The Int. J. Robot. Res.*, vol. 23, no. 2, pp. 155–165, 2004.

[30] R. Schuller, *et al.*, "Online learning of centroidal angular momentum towards enhancing dcm-based locomotion," in *Int. Conf. Robot. Autom.*, 2022, pp. 10 442–10 448.